Title
Characterizing unsaturated diffusion in porous tuff gravel

Authors
Hu, Qinhong
Kneafsey, Timothy J.
Roberts, Jeffery J.
et al.

Publication Date
2003-11-12

Characterizing Unsaturated Diffusion in Porous Tuff Gravel

Qinhong Hu[1,*], Timothy J. Kneafsey[2], Jeffery J. Roberts[1], Liviu Tomutsa[2], and Joseph S.Y. Wang[2]

[1] 7000 East Avenue, MS L-231

Lawrence Livermore National Laboratory

Livermore, CA 94550

[2] 1 Cyclotron Road, MS 90-1116

Lawrence Berkeley National Laboratory

Berkeley, CA 94720

Revised For:

Vadose Zone Journal

February 19, 2004

[*]Corresponding author (phone: 925-422-6774; fax: 925-422-3160; email: hu7@llnl.gov)

ABSTRACT

Evaluation of solute diffusion in unsaturated porous gravel is very important for investigations of contaminant transport and remediation, risk assessment, and waste disposal (for example, the potential high-level nuclear waste repository at Yucca Mountain, Nevada). For a porous aggregate medium such as granular tuff, the total water content is comprised of surface water and interior water. The surface water component (water film around grains and pendular water between the grain contacts) could serve as a predominant diffusion pathway. To investigate the extent to which surface water films and contact points affect solute diffusion in unsaturated gravel, we examined the configuration of water using x-ray computed tomography in partially saturated gravel, and made quantitative measurements of diffusion at multiple water contents using two different techniques. In the first, diffusion coefficients of potassium chloride in 2–4 mm granular tuff at multiple water contents were calculated from electrical conductivity measurements using the Nernst–Einstein equation. In the second, we used laser ablation with inductively coupled plasma–mass spectrometry to perform micro-scale mapping, allowing the measurement of diffusion coefficients for a mixture of chemical tracers for tuff cubes and tetrahedrons having two contact geometries (cube-cube and cube-tetrahedron). The x-ray computed tomography images show limited contact between grains, and this could hinder the pathways for diffusive transport. Experimental results show the critical role of surface water in controlling transport pathways and hence the magnitude of diffusion. Even with a bulk volumetric water content of 1.5%, the measured solute diffusion coefficient is as low as 1.5×10^{-14} m^2/s for tuff gravel. Currently used diffusion models relating diffusion coefficients to total volumetric water content inadequately describe unsaturated diffusion behavior in porous gravel at very low water contents.

INTRODUCTION

Studies of flow and transport in gravels have recently received attention because of the importance of gravel aquifers, the need to understand contamination characterization and remediation of gravel deposits in the vadose zone, and the use of gravel as capillary barriers for waste isolation. As stated in Tokunaga *et al*. (2003), relatively little information is available on the unsaturated hydraulic properties of gravels; this is also true for transport processes in unsaturated gravel systems. Conca and coworkers published pioneering work examining chemical diffusion behavior in porous gravels, yet this work was conducted more than ten years ago (Conca, 1990; Conca and Wright, 1990; Conca and Wright, 1992). With the improved understanding of water distribution in gravel, there is a strong need to investigate the diffusion processes in unsaturated porous gravel by employing the latest developments in instrumentation and techniques. Improved understanding of unsaturated diffusion in gravel will help in the characterization and remediation effort in gravel deposits at the Hanford Reservation (Washington). It will also help in the invert diffusion barrier concept for the potential underground high-level radioactive waste repository at Yucca Mountain, Nevada, where tuff gravel has been considered as an invert material (material filling the bottom of a tunnel having a circular cross section) to contain radionuclide transport.

The invert placed between the waste package/drip shield and the tuff host rock at Yucca Mountain is an integral component of repository performance. If effective, an invert diffusion barrier (caused by slow radionuclide diffusion through the invert) can greatly enhance waste-isolation capacity. Conca and Wright (1992; 2000) measured effective diffusion coefficients (D_e) in unsaturated soil, gravel, bentonite, and whole rock over a wide range of volumetric water contents; this free water content does not include interlayer water in clays or other structural water (Conca and Wright, 2000). They found that D_e values in all media were primarily a function of volumetric water content and not material characteristics. CRWMS M&O (2000b) reported that this diffusion data set was well correlated in terms of a power-dependence (Archie's law type) on the volumetric water content, and used a resultant "universal" power function to represent diffusive transport of radionuclides through the invert. However, in waste emplacement drifts, characterized by a humid environment with or without the presence of liquid water, crushed porous rock may provide unique characteristics that vary greatly from this generic power function (Wang *et al*., 2001; Hu and Wang, 2003). For example, Conca (1990) placed four different size fractions of tuff gravel samples (2–4 mm, 4–6.3 mm, 6.3–9.5 mm, and 15–25.4 mm) for equilibrium inside a chamber with a nearly 100% humidity atmosphere. After equilibrating about 70 days, all samples of individual grains were observed to be dry, despite the 2.7% intragranular water content. No electrical conductivity could be measured on these samples, resulting in an inferred diffusion coefficient below 10^{-15} m^2/s, which is the detection limit reported by Conca (1990) using electrical conductivity (EC) for estimating the diffusion coefficient. The inferred low diffusion value of 10^{-15} m^2/s at this water content deviates significantly from the "universal" power function with a diffusion coefficient (about 2.8×10^{-12} m^2/s), which is obtained with continuous fluid introduction. In other words, at the same water content, diffusion in samples prepared using high-humidity (without fluid source contact) is almost three orders of magnitude lower than in the samples prepared with liquid-water introduction.

This diffusion behavior is caused by the water distribution exhibited by porous-rock gravel (Figure 1). Rock surfaces in partially saturated environments will generally be wetted by liquid films that can be held either by adsorptive forces on mineral surfaces or by capillary forces in surface depressions. For a porous-rock-gravel system, the total water content is comprised of surface (intergranular) water (surface film water around grains and pendular water between rock grain contacts) and interior (intragranular) water (water contained within the rock matrix pores). Small pores and the relatively large porosity of tuff gravel could play an important role in retaining water in the internal pores, reducing the surface water content of the gravel to levels where diffusion becomes as low as the detection limits of conventional methods. On the other hand, the interior water is not likely to contribute significantly to water flow and transport in the unsaturated gravel system (Conca and Wright, 1990; Tokunaga *et al*., 2003). Pendular water elements between gravel grains serve as the bridging pathways between grains and control the efficiency of the system in attaining the upper limit of transport determined by surface films. At low water contents, diffusion in rock gravel could be very slow, because water films on surfaces can be discontinuous or absent. Conca and Wright (1992) reported an experimental method to determine diffusion coefficients (using the Nernst–Einstein equation) by using an unsaturated-flow apparatus in combination with electrical-conductivity measurements. However, experimental limitations may exist with this approach, such as the contact resistance at low water contact and the applicability of the Nernst–Einstein equation in geologic media at very low saturation. To further understand and explore the low diffusion potential in unsaturated porous gravel, we need to refine available testing methods or develop innovative approaches to measuring diffusion.

EXPERIMENTAL APPROACH

In this work, we (1) used x-ray computed tomography (CT) to examine the flow characteristics and water distribution in a tuff gravel column, (2) employed an electrical conductivity approach to measure the effective diffusion coefficient of similar gravel columns, and (3) examined diffusion behavior of single tuff grains with two contact geometries inside several humid environments. For this single-grain study, we employed a micro-scale mapping technique that involved using laser ablation interfaced with inductively coupled plasma–mass spectrometry (LA–ICP/MS).

Tuff block samples from the Topopah Spring welded (TSw) volcanic tuff, the potential repository geologic unit, were collected at the underground tunnel at Yucca Mountain, Nevada. For gravel column experiments, tuff samples were crushed and sieved into various-sized fractions. For the micro-scale mapping approach, tuff samples were machined into two shapes: cubic (1.50 cm in length) and tetrahedral (1.50 cm each side of the triangle and 1.30 cm in height). The external surface roughness of these machined samples was measured using a scanning white interferometer (Zygo Newview 200, Zygo Corporation, Middlefield, CT). The measured value of the root-mean-square (RMS) roughness is 2.2 μm over 714 μm scans.

X-Ray Computed Tomography Scanning of Tuff Gravel System

CT scanning provides a direct view of fluid distribution in geological media. Recently, Polak *et al*. (2002) used an x-ray CT scanner to investigate the diffusion of NaI between a fracture and the surrounding matrix under a saturated chalk core. Interested readers are referred to the paper of Clausnitzer and Hopmans (2000) for an excellent review about the background and principles of CT with respect to its application in flow and transport studies.

We used CT scanning to provide a preliminary evaluation of our conceptual model about moisture distribution and flow pathways in unsaturated tuff gravel. Using the CT scanner, we were able to observe pathways available for diffusive transport. A modified medical-based x-ray CT scanner with cross-sectional resolution of about 0.2 mm by 0.2 mm (Siemens Somatom HiQ, Siemens, Malvern, PA) was used to monitor moisture distribution in sample holders packed with crushed tuff. A high-accuracy (±12 μm) computer-controlled table was used for sample positioning (Tomutsa *et al*., 1992). This positioning table enabled back-and-forth movement of the sampler holder during the scanning process. Rapid, accurate, and repeatable positioning of the sample within the x-ray beam could be programmed to perform automated series of scans. The sample holder was constructed out of Plexiglas, had a 6.35 cm inner diameter (i.d.), 1.27 cm thickness, and was threaded at both ends.

Two different size fractions of tuff gravel, 16−25 mm and 6.3−9.5 mm, were used. The tuff gravels were initially oven-dried at 60°C for seven days to achieve a constant weight (change between two consecutive weighings < 0.01%). A drying temperature of 60°C was selected to remove pore water while keeping structural water of the samples (Soeder *et al.*, 1991). After packing the sample in the holder, a background set of scans was performed for the dry gravel. The sample holder was placed horizontally on the CT positioning table, and cross-sectional slices were acquired along the core, using an x-ray beam energy of 133 keV with a slice thickness of 1 mm. The sample and holder were fixed on the table during the experiment, ensuring proper registration of the CT images at precisely the same locations. Scans were performed consecutively for a total length of 3 cm at the middle section of the column. The 6.3−9.5 mm sample was then saturated by pumping Nanopure water (Barnstead International, Dubuque, IA) into the holder. Air escaped through a small hole on the top of the sample holder. The samples were submerged for a day, and then water was drained from a hole on the bottom side. When only about one third of the bottom section of tuff gravel was saturated, another series of scans was performed at the same locations. The difference between the wet and dry scans at each slice was used to determine the moisture distribution within the sample.

Diffusion Measurements by the Electrical-Conductivity Method

Diffusion of radionuclides in unsaturated gravel could occur (1) through water films (present on the gravel surfaces), (2) through water in the interconnected porosity (present within the gravel grains), or (3) very slowly on the solid mineral surface. Measuring low diffusion coefficients requires long duration measurements, the ability to sample on extremely small spatial scales, or an indirect approach. Calculating diffusion coefficients based on electrical conductivity measurements is an indirect technique that has been accepted for diffusants in bulk aqueous samples (Conca and Wright, 1992). The Nernst-Einstein equation relates the electrical conductivity of a solution to the effective diffusion coefficient of an ionic diffusant:

$$D_e = \frac{RT}{F^2}\frac{\delta Gt}{ZC} \qquad (1)$$

Here, R is the universal gas constant, T is the absolute temperature, F is Faraday's constant, δ is the geometric factor of the experimental cell, G is the measured conductance, t is the transference number, Z is the valence of the diffusant, and C is the diffusant molar concentration.

To use this method for inference of diffusion coefficients, we must account for sources of conductivity in our system. Our dry porous tuff was quite resistive, as was our sample holder. Thus, we consider the connected aqueous pathways (films in particular) in an unsaturated porous medium as the only electrical-current-carrying routes. We can measure a resistance and calculate the diffusion coefficient. This method directly accounts for the tortuosity of the fluid pathway on the gravel surface and the diffusion resistance at intergranular contacts.

A cell with four electrodes was constructed to contain tuff gravel and isolate the sample from the atmosphere (Figure 2). The 6.22 cm inner diameter cell was constructed out of transparent polyvinyl chloride (PVC) pipe. Nylon endcaps were machined such that two O-rings were placed between each endcap and the PVC pipe, and each endcap was fitted with a stainless-steel electrode to make contact with the sample across the entire cross-sectional area of the pipe. Two stainless-steel screen electrodes were placed in the center of the cell approximately 65 mm apart. A sealable access port was placed between the two screen electrodes.

The crushed tuff used in the measurements was from the 2–4 mm fraction of tuff sample, with internal porosity and grain bulk density of 10.5% and 2.23 g/cm^3 respectively. The grains were shard-like, often with one dimension greater than 4 mm. The tuff was somewhat friable, and some grain breakage was observed during normal laboratory handling.

The crushed tuff was vacuum saturated in 0.5 g/L (6.7 m*M*) KCl solution. The three compartments of the cell were filled with crushed tuff at the desired volumetric water content, ranging from fully saturated to about 10% saturation for tuff grains. Tuff was compacted into each of the three cell compartments, and the sliding endcaps were clamped together forcing contact between the tuff and electrodes. The porosity in each compartment was assumed to be equal. High water contents were initially used (saturated and initial drainage), and these were attained by emplacing the saturated tuff in the cell and draining the sample, using a porous ceramic drain in the cell. Further tuff drainage was accomplished using an ultracentrifuge (Beckman Model L8-60M/P, Beckman Coulter, Fullerton, CA). To do this, portions of the saturated tuff were placed in centrifuge cups and drained under specified conditions. Following the centrifugation, the tuff was placed into the cell inside a glove bag maintained at high relative humidity by a beaker of warm water. This was to prevent dryout of the surface layer of water on the tuff grains. Although all work was performed at normal laboratory temperatures, the filled cell was placed into an incubator maintained at 22 ^{o}C for several hours prior to measuring resistance, to allow for thermal equilibration.

Resistance measurements were made using a GenRad 1692 Digibridge LCR meter (QuadTech, Maynard, MA). The LCR meter was checked against many resistance measurement systems and found reliable for the expected conditions. Prior to making measurements, the meter was calibrated and the offset corrected to zero, according to the manufacturer's instructions. The four electrodes from the cell were connected to the four ports of the meter, and resistance (series) was recorded for the five frequencies generated by the meter (100, 120, 1,000, 10,000, and 100,000 Hz). For high water contents, measurements were made primarily at 1,000 Hz, because the quality factor (Q) indicated by the meter was low. (Q provides an indication of the phase shift [Q = tan (phase shift)] between the current and voltage measurement.) The Nernst–Einstein equation requires the passive resistance (phase shift=0), thus the resistance value for the frequency with the lowest Q was selected for diffusion coefficient calculation. In many cases, alternate electrode configurations were connected to the meter, and the resistance was recorded. Using the electrode numbers from Figure 2, we made measurements for some water contents in the 1144, 1122, 2233, 3344, 1234 (four electrode), 1133, and 2244 configurations, where (for example) 1144 indicates that Current+ was connected to electrode 1, Potential+ to electrode 1, Potential- to electrode 4, and Current- to electrode 4. Because both positive connections were connected to one electrode and both negative connections were connected to another electrode, we call this a two-electrode measurement. This allowed for an analysis of two- and four-electrode measurement techniques.

Diffusion Measurements by the Micro-Scale Mapping Method

Laser ablation refers to the process in which an intense burst of energy delivered by short laser pulses is used to vaporize a minute sample (in the range of nanograms) from a specific location of a sample. The chemical composition of the vaporized sample is then analyzed with inductively coupled plasma-mass spectrometry (ICP-MS). Laser ablation, coupled with ICP-MS (LA/ICP–MS), has recently evolved as a powerful analytical tool for solid sampling (Russo *et al.*, 2000). LA/ICP–MS can determine simultaneously a large number of chemical elements with very low detection limits. The high spatial resolution (in the range of microns) achieved by a focused laser beam makes LA/ICP–MS a very attractive tool for slow diffusion processes.

A detailed study, reported in Hu *et al*. (2001), was conducted to evaluate the potential of the LA/ICP–MS approach to direct measurement of diffusion coefficients, both at rock surfaces and the interior of rock matrix. The study included choosing appropriate tracers, probing elements intrinsic to tuff that can serve as internal standards to correct for different LA/ICP–MS conditions, and evaluating the mapping technique.

We used a laser ablation system (CETAC LSX-200, CETAC Technologies, Omaha, NE) interfaced with an ICP-MS (VG-PQ3 Spectrometer, VG Elemental, Franklin, MA) with a range of spot sizes (ranging from 25 μm to 350 μm). The spot size dictates the spatial resolution during the surface mapping, and number of laser pulses determines the amount sampled; a combination of spot size and number of laser pulses could be made to meet different research objectives. A smaller spot size will, under the same number of laser pulses, sample less solid material, leading to lower analytical precision. Additionally, for heterogeneous samples, using a smaller spot results in more observed heterogeneity. The tuff consists largely (~99 vol. %) of the former glassy matrix now devitrified to fine crystals of cristobalite, alkali feldspar, and quartz of 3-10 μm size fractions, as shown from the scanning electron microscopy analysis (Johnson *et al*., 1998). We primarily used a medium spot size (100 or 200 μm) for representative sampling, with measured relative standard deviation about 10-15%.

Evaluation from many tests indicates that, among all the intrinsic tuff elements, aluminum (Al) consistently exhibits the best signal stability (i.e., least heterogeneity). Therefore, we use Al for the ratio approach (dividing the response of the element of interest [the tracer chemical in this case] by the response of Al) to provide a normalized response that corrects any uncertainty related to LA/ICP–MS. This uncertainty could include, for example, less mass ablation as the sampling depth increases or possible energy fluctuations of the laser. To investigate the effect of intergrain contact and relative humidity (hence thickness and continuity of surface water films), we designed diffusion measurements with contact treatments of different rock-grain geometries (cube and tetrahedron) inside several RH chambers (43, 76, 93, 98, and nearly 100%). The RH values of 43, 76, 93, and 98% were controlled and maintained with saturated salts of K_2CO_3, NaCl, Na_2SO_4, and $CaSO_4$, respectively. The higher (near 100%) relative humidity was maintained by the evaporation from water beakers inside the enclosed chamber. Different intergrain contact points will help us understand the role of pendular water elements and water film continuity in affecting/controlling diffusion pathways. A range of RH conditions were used to simulate the scenarios of transient RH environments inside the drifts following the emplacement of waste packages. Both water film thickness and continuity are closely related to RH conditions and hence to potential diffusive radionuclide transport.

A half-element (source-sink) approach was used for diffusion measurement of unsaturated tuff gravel (Figure 3). The half-element design is based on the half-cell concept, wherein each cell is of the same geometry, which is commonly used for diffusion measurements (Shackelford, 1991; Flury and Gimmi, 2002). In the half-element approach, a source element (a tuff cube in this work) containing a tracer was placed in contact with a sink element (either a cube or a tetrahedron) not containing the tracer, both under the same temperature and RH. The tracer will then diffuse from the tracer-containing element to the other, and its diffusion coefficient is obtained from the concentration profile at different locations at a certain diffusion time.

The source tuff cube was vacuum-saturated with a tracer mixture solution that contained bromide (Br^-) and perrhenate (ReO_4^-). Both species act as nonsorbing tracers, confirmed from our laboratory column transport experiments using crushed tuff. Perrhenate serves as an analog to technetium (Brookins, 1986), which in the form of pertechnetate ($^{99}TcO_4^-$) is of concern for the potential repository at Yucca Mountain. Cationic sorbing tracers Cs^+, Co^{2+}, Sr^{2+}, and Sm^{3+}, as the counter ions for the nonsorbing anions in the tracer solution, were chosen to examine the combined transport from unsaturated diffusion and retardation. This paper is, however, focused on the behavior of nonsorbing tracers.

The sink element was also vacuum-saturated, but without tracers. Source and sink elements were then separately placed inside a humidity chamber within an incubator maintained at 22°C. Cube weight was periodically monitored until it reached a constant weight. This pre-equilibration, which took 137 days for the lowest RH (43%), was to ensure similar water potential was established between source- and sink-elements to prevent/minimize potential advective transport. The elements were then placed in a customized sample holder, clamped together, and placed in the RH chamber to start the diffusion test (Figure 3). For the cube-tetrahedron geometry, a cube face was in contact with an apex of the tetrahedron, resulting in a point contact between the elements. After a certain diffusion duration, the diffusion test was stopped by separating the source and sink elements. Tracer distributions on the surface of the sink element were immediately mapped using LA/ICP–MS. After mapping the sink cubes, a small groove was hand-sawed in the middle of the top face parallel to the diffusion direction, and the cube was cracked open with a hammer and a chisel to expose the interior. The interior surface was then mapped by adjusting the laser focus at each sampling location for the exposed rough surface. Stable responses were obtained during testing of these tuff elements despite the rough surface (Hu *et al*., 2001).

RESULTS AND DISCUSSION

CT Imaging of Tuff Gravel

Figure 4 shows twelve consecutive 1 mm thick cross-sectional images for 16−25 mm and 6.3−9.5 mm tuff gravels. Very little physical contact is observed between the tuff grains for the 16−25 mm size fraction, while noticeable, limited contact exists for the smaller size gravel. The measured bulk density was 0.549 and 0.806 g/cm^3 for the columns packed with 16−25 mm and 6.3−9.5 mm gravels, respectively. Transport pathways in such gravel systems could be potentially hindered because of the limited number of contact locations between grains.

A series of CT images are shown in Figure 5a for partially saturated 6.3−9.5 mm gravel. Water pockets (purple color in Figure 5a) are easily discerned in the scans from air and tuff grains. Subtraction of a set of dry scans from the wet background scans is shown in Figure 5b to indicate the water distribution. In these images, only the difference between the two conditions (dry and wet) is observed. Some water is shown in the nonsubmerged top part (Scan No. 1 of Figure 5b), and this is probably caused by the water pooling on the top of the flat grains. Also, tuff grains in the top portion are not totally subtracted out, probably because of the slight movement of grain position during water introduction and drainage. A slight positioning error is also apparent as the sample holder outline is slightly visible. Outlines of individual grains may be enhanced similarly.

Diffusion Measurements by the Electrical Conductivity Method

Measured diffusion coefficients

We measured the resistance of partially saturated crushed tuff gravel occupying a cell with known dimensions. The tuff was conditioned with preset water contents and the water contained a known concentration of potassium chloride. Using the measured resistance and known geometry, we calculated effective diffusion coefficients D_e (L^2 T^{-1}), which incorporates the effect of the geometry of the grains and their contacts, and the liquid content of the unsaturated system on diffusion.

The diffusion coefficients calculated using the Nernst–Einstein equation for volumetric moisture content are shown in Figure 6 and Table 1. The five points with volumetric water content greater than 5.4% were attained by drainage of the initially brine saturated cell. Lower volumetric water contents were achieved by centrifuging vacuum-saturated tuff at 1,000, 2,000, 3,000, 4,000, and 8,000 revolutions per minute (rpm) in an ultracentrifuge (10-20 minutes, with a consistent time used for each speed) prior to placing it in the cell. These speeds correspond to relative centrifugal forces of 45, 181, 408, 726, and 2,903 g. The cell was allowed to equilibrate for several hours in an incubator at 22 ^{o}C prior to measurement. The tuff surface appeared to become progressively drier as the centrifuge speed increased. Any handling of the tuff resulted in some breakage. Centrifugation at 8,000 rpm resulted in a high amount of smaller particles being generated (and a higher packing density in the cell), which could result in a higher diffusion coefficient. In a similar study, tuff was also observed to disintegrate, with sharp angular points breaking down, at centrifuge speeds larger than 6,000 rpm (CRWMS M&O, 2000a).

The calculated diffusion coefficients were compared to those presented by Conca and Wright (1990) and to the data presented by OCRWM M&O (2000a), all obtained from EC measurements. At moisture contents larger than 5.5%, our results agree very well with previous measurements and the power-law-curve fit. However, at lower moisture contents, our results tend steeply towards lower diffusion coefficients than the power-law curve fit. In our measurements, the lowest volumetric water content we achieved was about 5% (on a cell volume basis). The volumetric water content declined only slightly on a tuff grain basis as the centrifuge speed was increased for enhanced drainage. It is probable that this slight reduction in water content comes from the surface films and pendular elements. These slight changes, however, resulted in an increased measured resistance and a decreased calculated diffusion coefficient, without any apparent decrease in volumetric water content (cell basis). This is consistent with the unique behavior of water distribution in porous tuff, as discussed above.

Evaluation of the electrical conductivity approach

Extending the application of the Nernst–Einstein equation to diffusion in unsaturated porous media requires several assumptions. We first must assume that the water films are thick enough to act as bulk water. Nearest the mineral surface, the water molecules will be relatively fixed (unlike bulk water). Ions opposite in charge to the surface charge will be concentrated near the surface, while similarly charged ions will be repelled from the surface. In very thin water films, both of these layers will be compressed towards the mineral surface. The higher viscosity of the water molecules on the solid surface will lead to slower diffusion, because the diffusivity of ions in water is inversely proportional to the viscosity of the water. Kemper (1960) showed that the viscosity of the first three layers of water sorbed on Na-saturated mineral surfaces was about 10, 1.6, and 1.1 times, respectively, that of bulk water. van Olphen (1965) (cf., Stewart, 1972) reports that for montmorillonite the matric potentials needed to desorb the fourth, third, second, and first layers of adsorbed water are about 200, 1,200, 2,500, and 5,400 bars respectively. Stewart (1972) extrapolated the fifth and sixth layer of adsorbed water to be in the region of 30 to 50 bars. The equivalent matrix potential under our centrifugation condition at 8,000 rpm is 13.4 bars; therefore, the effects of water structure on slow diffusion are not expected to be significant.

One important requirement for the use of the Nernst–Einstein equation is that the mode of electrical conduction must be known. That is, to use the Nernst–Einstein equation to calculate diffusion coefficients in an aqueous system, there must be an understanding of the contribution to total electrical conduction from various possible modes of current conduction. If modes of current conduction other than through water are present, such as through mineral lattices, along the dry mineral surface, through adsorbed water on the mineral surface, through air in the intragranular pore space, or at the grain/grain connections, the Nernst–Einstein equation may not be applicable, or these individual effects may require quantification. Our system used a hydrophobic, resistive sample holder, and the resistivity of air, silicate minerals, and tuff glass is high, allowing us to eliminate these current pathways. Attempts to measure the resistivity of air-dry tuff failed because of the high resistivity, leaving bulk water and surface water conduction as the only conductivity pathways.

Other concerns include electrode design, electrode/sample polarization, and contact impedance at the electrode/sample interfaces. These problems can be minimized by constructing optimally sized and shaped sample holders and by performing experiments on samples in which electrode spacing is the only variable. We assess the effects of electrode-contact impedance by making measurements with a four-electrode configuration and multiple two-electrode configurations. When a four-electrode configuration is used, current is applied across the outer electrodes and potential is measured across the inner electrodes. In the wires and electrodes, current is carried by electrons; in the water-rock system, current is carried by ions. This change in charge carrier from electronic to ionic occurs at the current electrode/rock interface and results in contact impedance. The inner electrodes measure only the potential, and since very little current is drawn from the system to make this measurement, there is no contact impedance at these electrodes. Calculating the resistance between the potential electrodes can then be accomplished without the influence of contact impedance. Using the two-electrode configuration, current is applied and potential is measured at the same two electrodes. Thus, any contact impedance is included in the resistance calculation. This contact impedance was minimal at high volumetric water contents, but increased to as much as 5% of the indicated resistance in the drier measurements. However, the effect of surface water connectivity on diffusion is so predominant that such refinement yields similar results (shown in Figure 6), to those done by others in which a two-electrode design is used.

An additional concern with electrode-sample contact is that for the Nernst-Einstein equation to apply, a passive resistance (near-zero phase angle) was required. As the sample water content changed, the frequency providing the most passive resistance (smallest phase angle) also changed. Conca and Wright (1992) used a fixed impedance of 1,000 Hz for their two-electrode configurations. For most of our two-electrode measurements, we confirmed that 1,000 Hz was the best of the five frequencies available on the GenRad 1692. For the four electrode measurements, however, 100 and 120 Hz provided more passive resistances. The geometry of the measurement cell also affected the phase shift. Values of Q close to zero were obtained across a wider frequency range (1,000 Hz–10,000 Hz) for the two electrode measurements across the entire cell, whereas for the shorter intervals, frequencies near 1,000 Hz were required.

It is appropriate to ask what effects grain size and internal porosity have. The effect of grain size has not been adequately investigated. All of our specimens had nominally the same grain size. Much larger volumes would be necessary for larger gravel sizes. With these larger grain sizes, it would be difficult to establish the appropriate moisture conditions and representatively measure both resistance and physical properties to the accuracy needed. An ultracentrifuge might limit preparation to three grains at a time, and the use of relative humidity chambers would require the very slow transfer of large amounts of mass. Under similar thermodynamic conditions, smaller grains provide larger surfaces. If we assume that the surface film controls the electrical conduction (and thus the diffusivity), smaller grains should provide less diffusive resistance.

Diffusion Measurements by the Micro-Scale Mapping Method

Evaluation of testing technique

During our preliminary experiments for measuring unsaturated diffusion in a cube-cube configuration in a nearly 100% RH environment, the diffusion time used was as long as 150 days, based on our sample length (1.5 cm) and a diffusion coefficient of smaller than 10^{-15} m^2/s, as inferred by Conca (1990) from the resistance detection limit. Our measurements of tracer concentration indicate that diffusion coefficients are much higher than this inferred value under similar RH conditions.

Figure 7 shows the tracer distribution and comparison for both the source and sink cubes from an experiment in which two cubes were placed side by side in a nearly 100% RH container for 150 days. In this figure both the x- and y-axes for the all plots have the same scale to facilitate the comparison. Nonsorbing tracers ($Br^-$and ReO_4^-) are evidently present across almost the entire sink cube face (Face 3) perpendicular to the interface face (in the direction of surface diffusion) after 150 days' diffusion time. The distribution of diffusive tracers is corroborated from the results on the far-side face of the sink cube, where both $Br^-$and $ReO_4^-$are detected. As expected, the tracer distributions on the far-side face of the source cube are more uniform and at much higher (about 10 times) concentrations than the sink cube. Furthermore, the interface faces have similar tracer concentration distributions for both the source and sink cubes, indicating good contact and diffusive mass transfer between cubes.

Measured diffusion coefficients

An appropriately short diffusion time was then selected for different experimental setups, with longer time for lower RH tests (Table 2). Figure 8a shows the mapped tracer distribution for cube-cube configuration exposed to a 98% RH environment, which exhibits a typical diffusion profile across the interface (X=0 cm). Intensity of tracer response is plotted in log scale on the Y-axis, contrary to the typical diffusion profile in arithmetic scale reported by others, because of the high sensitivity of ICP/MS. It appears that the diffusion front reaches about 1 cm and 0.1 cm for both tracers in the 98% RH and 43% RH tests, respectively. After this distance, the signals essentially show the background response. The background response for Br^- is higher than that for ReO_4^-, because of its lower sensitivity by ICP/MS analysis. Nevertheless, we obtained a diffusion profile with a signal spanning more than two orders of magnitude for Br^-, compared to three orders for ReO_4^-, to provide us with a high-resolution value of the diffusion coefficient obtained from the profile.

In the half-element configuration and for an infinite system in which the concentration profile does not reach the ends of the element, the analytical solution to the transient diffusion equation (Fick's second law) is as follows (Crank, 1975; Flury and Gimmi, 2002):

$$\frac{C}{C_0} = \frac{1}{2} erfc \frac{x}{2\sqrt{D_e t}} \qquad (2)$$

where C (M L^{-3}) is the observed concentration at location x based on an initial concentration C_0 (M L^{-3}), x (L) is the distance from the interface boundary into the sink element, and t (T) is the diffusion time.

Figure 9 shows examples of curve-fitting of the obtained tracer concentration profiles; with Figure 9a presenting a sensitivity analysis of varying D_e. The fitted diffusion coefficients for different half-element configuration and RH environments are listed in Table 2. The diffusion of

Br^- is relatively faster than ReO_4^-, as expected from its larger aqueous diffusion coefficient (D_0); 2.08×10^{-9} m^2/s for Br^- and 1.46×10^{-9} m^2/s for ReO_4^- (Lide, 2000). The ratio of measured D_e for Br^- to ReO_4^- is also presented in Table 2, with an average of 1.81 and a standard deviation of 0.65 for our 11 measurements, compared to the D_0 ratio of 1.42. The averaged ratio for seven surface diffusion measurements (D_{Br-}/D_{ReO4-}) is 1.59 with a standard deviation of 0.38. The similarity between the ratios from tuff and aqueous solution confirms that diffusion is the predominant, and likely the only, mode of transport in our experimental systems, as we intended to achieve. For cube sinks, a boundary zone of a few millimeters appears to exist (Figure 9a) with a lower concentration (higher diffusion) than the overall pattern. This might be related to the boundary condition of the half-element configuration wherein diffusion is not of one-dimensional. We do not see such an edge effect for the cube-tetrahedron contact, as the fitted diffusion curve based on one-dimensional Equation 2 captures all data very well for tetrahedral sink sample (Figure 9b).

Using multiple RH to establish moisture content provides us with multiple water saturations and a relevant scenario to the waste package emplacement drifts. The bulk liquid saturation, and hence volumetric water content, is closely related to the RH environment. As the RH decreases, the diffusion coefficient decreases dramatically (Table 2). At water contents about 10%, the measured data start to deviate from the "universal" power-law fit for diffusion as a function of water content. The deviation is more pronounced at the lower RH treatments, though the bulk water contents are still high (Figure 6). The two approaches, EC and micro-scale mapping, give overlapping diffusion coefficients. The advantage of the EC method is that it provides a relatively fast measurement of diffusion as a function of water content. The micro-scale mapping approach complements with the EC technique in obtaining a diffusion value as low as 10^{-14} m^2/s under lower water contents.

Hu and Wang (2003) reviewed the behavior of, and relationship between, nonsorbing diffusants and water content, particularly for porous aggregates (rock gravel). Diffusion is monotonically related to water content, but the relationship is not simple and depends upon the range of water content (in other words, different forms of relationships at different water-content ranges). The relationship is also related to the texture and characteristics (such as surface wettability) of the geologic medium. It is evident that the water content at which deviation occurs is different among the tuffs and silica sand (Figure 6), which is probably related to the sample size used and the difference in porosity and surface wettability. At some low water content, the diffusion pathways become disconnected and diffusion effectively stops. Using continuum percolation theory, Hunt and Ewing (2003) interpreted the phenomenon of vanishing solute diffusion at threshold water content in porous media.

Surface diffusion

In our investigations, we used 10 or 20 laser pulses to map tracer concentration distributions at different locations. A single laser pulse creates a crater with a depth of about 0.83 μm, obtained from multiple measurements using a polished tuff sample with a RMS surface roughness of 0.28–0.35 μm (from four 714 μm long scans). Twenty laser pulses, having a corresponding sampling depth about 16 μm, were used for the tracer mapping on the gravel surface from which the diffusion coefficients was obtained in Table 2. The unpolished tuff elements used in the diffusion tests have a measured surface roughness about 2.2 μm, which indicates the topographic constraint on water film thickness (Tokunaga *et al*., 2003).

Tokunaga and coworkers used a synchrotron x-ray fluorescence technique, which has a quantification limit of 0.3 μm, to measure a range of water film thickness for glass, natural rock and gravel samples. Tokunaga and Wan (1997) reported that an average surface film thickness for a Bishop Tuff fracture surface with a roughness ~50 µm ranged from 2 to 70 µm at matrix potential greater (more positive) than about –250 Pa (with corresponding RH >99.999%, according to the Kelvin equation). The average film thickness on a roughened glass (with a surface roughness of about 9 µm) was between 1.0 µm to 2.3 µm (Tokunaga *et al.*, 2000). This was measured under matric potentials of –20 kPa and –1.2 kPa, which correspond to RH exceeding 99.9%. With gravel samples from Hanford, Washington, Tokunaga *et al.* (2003) reported average film thicknesses of 7–10 µm at near-zero (-0.05 to -0.10kPa) matric potentials. Under drier conditions, they expect that the smooth surfaces of natural Hanford gravels cannot support thick (> 2 µm) water films for fast advective flow, and chemical transport will be diffusion-limited. Our diffusion experiments were conducted at drier conditions than reported above.

The effects of RH conditions and sample wettability (hydrophobicity) are very critical for surface film thickness and connectivity. Using an ellipsometric technique, Gee *et al.* (1990) determined the equilibrium water film thickness on quartz as a function of relative vapor pressure. (The natural crystalline quartz plates used were polished with a RMS surface roughness of 10 Å.) They also evaluated the effect of wettability of film thickness by dehydroxylating the quartz samples from heating treatments. Some of their results are reproduced here in Figure 10. It is not until the system nears saturation (RH>90%) that the film thickness undergoes a sharp increase indicative of the formation of multilayers of water on the quartz surface (Figure 10 a). In contrast, the magnitude of the film thickness on heat-treated quartz is much lower (Figure 10b). Another feature of the dehydroxylated quartz is that film thickness does not increase monotonically with RH, but seems to fluctuate and displays a distinct step at RH of 80%. The films are metastable at small film thickness (Gee *et al.*, 1990).

We are not aware of any reports on contact angle measurement for tuff samples at Yucca Mountain, but the tuff is water wetting because water drops immediately spread over the tuff surface. Our measured diffusion coefficients seems to decrease significantly at RH less than 93% (Table 2), similar to the deflection point of surface water film at 90% RH observed for the fully water-wetting quartz (Gee *et al*., 1990). In a lower RH environment, the diffusion coefficient becomes even smaller; the values are more than three orders of magnitude smaller at 43% RH than at 98% RH. This is likely related to the effect of surface film thickness on the magnitude of diffusion.

Furthermore, it seems that the decreasing surface diffusion from the less extensive surface water films is more critical than the extent of contact point. Surface diffusion values for both cube-cube and cube-tetrahedron contact at several RH conditions are presented in Table 2. At high RH environments (>76%), the surface diffusion on the cube-cube face contact is slightly greater than that on the cube-tetrahedron point contact. The interior diffusion is probably controlled by the pore-water type but diffusion needs to undergo tortuous pathways inside the tuff. At a lower RH of 43%, surface diffusion on the tetrahedron is somewhat greater than that on the cube surface and interior, possibly due to additional water at the cube-tetradedron point contact from the capillary forces.

Other resistivity measurements in the unsaturated tuff of Yucca Mountain lend evidence of water configuration at different saturations and its role in controlling flow pathways. Roberts and Lin (1997) reported water existing in three configurations as a function of water saturation. These configurations are adsorbed water on solid surfaces (Region 1, from completely dry to ~15% saturation), isolated pockets of water (Region 2, in the saturation range of ~15 to 35%), and continuous (bulk) water (Region 3, from ~35 to 100% saturation). Region 1 has the steepest drop in resistivity as saturation increases, and conduction is assumed to be primarily through layers of adsorbed water. We expect that this region corresponds to the threshold water content to support solute diffusion. From the measured porosity and surface area/volume reported in Roberts and Lin (1997), we calculate that the average water-film thickness is about 115 Å at the water saturation of 15%. This calculation supports the importance of a connected water film on resistivity and diffusion at this range of low water content. Region 2 is comprised of pendular rings at grain contacts and pore-throat constrictions. The transition from Region 2 to Region 3, which might correspond to RH >93% in this study, is less abrupt and indicates a gradual displacement of air in the pore space.

Interior diffusion

The interior diffusion could be composed of pore-water diffusion (diffusion in relatively large, interconnected water-filled pores and microcracks), grain-boundary diffusion (aqueous diffusion through relatively small pore spaces such as grain boundaries), or intracrystalline diffusion in minerals. Grain boundaries usually contain thin water films on their surfaces, and diffusion through thin intragranular water films in well-consolidated rocks is often much slower than pore-water diffusion because the structure of the thin water film may be more constrained from interaction with solids than “free” water in pores. From compiled literature data for many types of rock, Nakashima (1995) reported that grain-boundary diffusivity is less than 10^{-15} m^2/s, and the ratio of pore-water to grain-boundary diffusion is on the order of 100 to 1,000. However, Kozaki et al. (2001) reported that grain-boundary diffusion was the predominant diffusion process, even for anions like chloride, in saturated montmorillonite. Intracrystalline diffusion will be even slower because of the extremely constricted diffusion through narrow channels within the crystal structure. For example, Rundberg (1987) estimated, from kinetic sorption data, that intracrystalline diffusion coefficients in partially welded devitrified tuff from the Prow Pass unit at Yucca Mountain ranged from 1.1×10^{-19} to 6.7×10^{-17} m^2/s for cesium, strontium, and barium.

Some insights can be obtained from this study, as tracer concentrations for both surface and interior of the tuff are available for cube sinks. At high RH environments (>76%), the surface diffusion on the tuff consistently is slightly greater than interior diffusion. The interior diffusion is probably controlled by the pore-water type but diffusion needs to undergo tortuous pathways inside the tuff. At lower RH environments, there is little difference for the measured diffusion coefficients between the surface and interior, because of the reduced surface diffusion due to less-extensive surface films. For the interior diffusion, we speculate that the transition from pore-water diffusion to the grain-boundary diffusion occurs at these lower RHs. It is likely that the diffusion at 43% RH is predominantly influenced by the grain-boundary water.

The use of tracers with different molecular sizes helps us evaluate the steric hindrance effect on diffusion within narrow pores. This pore-size restriction effect is not evident among Br^- and ReO_4^-, with ReO_4^- being a larger molecule. In saturated rock-beaker diffusion tests measuring tracer concentration change in tuff cavity (beaker), Triay *et al*. (1997) suspected this exclusion effect for TcO_4^-. Instead of monitoring the concentration change in the liquid reservoir as in conventional diffusion tests, we directly measure the concentration of two diffusivity tracers in rock samples to examine the potential exclusion effect. A significant steric hindrance effect is expected when pore diameter is less than 10 times the molecular diameter (Grathwohl, 1998). Using mercury porosimetry, Roberts and Lin (1997) reported that the average matrix pore diameters (weighted by increments of pore space filled) for welded and densely welded Topopah Spring tuff samples at Yucca Mountain are 53.1 nm and 19.7–21.4 nm, respectively. From the weight-gain measurements on core saturation of densely welded TSw samples inside controlled relative-humidity chambers, we found that about 10% of tuff pores were smaller than 10 nm. The effective ionic diameters for Br^-, ClO_4^-, and TcO_4^- are 0.390, 0.472, and 0.480 nm, respectively (Neck and Kanellakopulos, 1987). Given its similar structure, the diameter of ReO_4^- is probably similar to ClO_4^- and TcO_4^-. Based on the above information, the pore-size restriction in the tuff matrix is not expected to have a significant impact on the diffusive processes for these tracers, as confirmed by experimental results.

CONCLUSIONS

In this work, innovative and complementary approaches are employed to investigate and characterize the unsaturated diffusion processes in porous gravel. At unsaturated conditions, aqueous diffusion occurs in liquid films on the gravel surfaces, and the diffusion will be very slow if the water film is thin and discontinuous. Diffusion in unsaturated gravel is not solely dependent upon the magnitude of water content; rather it is more closely related to the thickness, mobility, and continuity of the surface water. Within porous rock gravel, appreciable water can exist as a surface film around the grain without significantly contributing to overall diffusion, because this water is structurally constrained.

At Yucca Mountain, unsaturated porous tuff gravel could serve as a diffusion and transport barrier because of its water-distribution characteristics. While RH is low, such as the time period following heating phase from radionuclide decay, surface water films are expected to be thin, discontinuous, or completely removed. Diffusive transport of radionuclides in such systems will be greatly reduced. Additionally, the thermal history of a mineral affects its wettability, as quartz samples that have been heat to a temperature of 1,050 ^{o}C are more hydrophobic than nonheat-treated samples (Gee *et al.*, 1990). This thermal effect could impact diffusion through a gravel invert. Porous tuff gravel can, however, hold a considerable amount of water within grains because of its large capillary force. It can imbibe liquid from seepage or breached waste packages to minimize drainage of radionuclides through the invert gravel. This unique behavior of porous gravel can be harnessed to maximize the performance of the potential repository.

Currently used diffusion models relating diffusion coefficients to total volumetric water content inadequately describe the bimodal diffusion behavior in porous gravel at low water contents. The "universal" curve does not capture the unique characteristics of water distribution for gravel at water contents below about 9%. The distribution of water in gravel (containing both surface and interior water) is analogous to that of a fracture-matrix water system, and a dual-continuum approach could be used to model the diffusion behavior. Considering the importance and recent recognition of gravel in waste management and environmental remediation, such a dual-diffusivity model approach is necessary.

ACKNOWLEDGMENTS

This work was supported by the Director, Office of Civilian Radioactive Waste Management, U.S. Department of Energy, through Memorandum Purchase Order EA9013MC5X between Bechtel SAIC Company, LLC, and the Ernest Orlando Lawrence Berkeley National Laboratory (LBNL), and Lawrence Livermore National Laboratory (LLNL). The support is provided to LBNL through the U.S. Department of Energy Contract No. DE-AC03-76SF00098, and to Lawrence Livermore National Laboratory under contract No. W-7405-Eng-48. We greatly appreciate the help from Andrew Mei for rock machining, Ingrid Zubieta for laboratory assistance, Xiang-Lei Mao and Jhanis Gonzalez of LBNL for their insightful discussions and operation related to LA/ICP–MS, and Steven Carlson of LLNL for helpful discussions about electrical conductivity. The authors also thank Christopher Campbell and Daniel Hawkes of LBNL for many helpful comments. The authors greatly appreciate numerous inputs from James Conca and another anonymous reviewer that help improve the quality and presentation of this work.

REFERENCES

Brookins, D.G. 1986. Rhenium as analog for fissiogenic technetium: Eh-pH diagram (25 ^{o}C, 1 bar) constraints. *Appl. Geol.*, 1:513-517.

Clausnitzer, V., and J.W. Hopmans. 2000. Pore-scale measurements of solute breakthrough using microfocus X-ray computed tomography. *Water Resourc. Res.*, 36(8):2067-2079.

Conca, J.L. 1990. Diffusion barrier transport properties of unsaturated Paintbrush tuff rubble backfill. *Proceedings of the First International High-Level Radioactive Waste Management Conference*, 1: 394–401.

Conca, J.L. and J. Wright. 1990. Diffusion coefficients in gravel under unsaturated conditions. *Water Resour. Res., 26*(5): 1055–1066.

Conca, J.L. and J. Wright. 1992. Diffusion and flow in gravel, soil, and whole rock. *Appl. Hydrogeo.,* 1: 5–24.

Conca, J. L. and J. Wright. 2000. Aqueous diffusion in the vadose zone. *Vadose Zone Science and Technology Solutions*. pp. 796-797 B. B. Looney and R. W. Falta, Eds. Columbus, OH, Battelle Press.

Crank, J. 1975. *The Mathematics of Diffusion*. 2nd ed., Oxford University Press Inc., New York.

CRWMS M&O (Civilian Radioactive Waste Management System Management and Operating Contractor). 2000a. *The Determination of Diffusion Coefficient of Invert Materials*. TDR-EBS-MD-000002 REV 00. Las Vegas, Nevada.

CRWMS M&O. 2000b. *Invert Diffusion Properties Model.* ANL-EBS-MD-000031 REV 01. Las Vegas, Nevada.

Flury, M., and T.F. Gimmi. 2002. Solute Diffusion. pp. 1323-1351. Chapter 6.2 In *Methods of Soil Analysis*. Part 4 – Physical Methods. J.H. Dane and G.C. Topp (eds.). Soil Sci. Soc. Am., Madison, Wisconsin.

Gee, M.L., T.W. Healy, and L.R. White. 1990. Hydrophobicity effects in the condensation of water films on quartz. *J. Colloid Interface Sci.*, 140(2): 450–465.

Grathwohl, P. 1998. Diffusion in Natural Porous Media: Contaminant Transport, Sorption/Desorption and Dissolution Kinetics, Kluwer Academic Publishers, Boston, MA.

Hu, Q., T. Kneafsey, J.S.Y. Wang, J.J. Roberts, and S. Carlson. 2001. *Summary report on Phase 1 feasibility study of in-drift diffusion*. LBNL–49063, Lawrence Berkeley National Laboratory, Berkeley, CA.

Hu, Q., and J.S.Y. Wang. 2003. Aqueous-Phase diffusion in unsaturated geological media: A review. *Critical Reviews in Environmental Science and Technology*, 33(3):275-297.

Hunt, A. G. and R. P. Ewing. 2003. On the vanishing of solute diffusion in porous media at a threshold moisture content. *Soil Sci. Soc. Am. J.*, 67(6): 1701-1702.

Johnson, J.W., K.G. Knauss, W.E. Glassley, L.D. DeLoach, and A.F.B. Thompson. 1998. Reactive transport modeling of plug-flow reactor experiments: quartz and tuff dissolution at 240^{o}C. *J. Hydrol.*, 209: 81–111.

Kemper, W.D. 1960. Water and ion movement in thin films as influenced by the electrostatic charge and diffuse layer of cations associated with clay mineral surfaces. *Soil Sci. Soc. Am. Proc.*, 24:10-16.

Kozaki, T., K. Inada, S. Sato, and H. Ohashi. 2001. Diffusion mechanism of chloride ions in sodium montmorillonite. *J. Contam. Hydrol.*, 47: 159–170.

Lide, D.R. (Editor-in-Chief). 2000. *CRC Handbook of Chemistry and Physics*, 81st Edition. Boca Raton, Florida, CRC Press.

Nakashima, S. 1995. Diffusivity of ions in pore water as a quantitative basis for rock deformation rate estimates. *Tectonophysics*, 245(3-4): 185–203.

Neck, V., and B. Kanellakopulos. 1987. Partial molar volume and effective ionic radius of the TcO_4^- ion in aqueous solution. *Radiochim. Acta*, 42:135-137.

Polak, A., R. Nativ and R. Wallach. 2002. Matrix diffusion in northern Negev fractured chalk and its correlation to porosity. *Water Resourc. Res.*, 268:*203-213.*

Roberts, J.R., and W. Lin. 1997. Electrical properties of partially saturated Topopah Spring tuff: Water distribution as a function of saturation. *Water Resour. Res.*, 33(4): 577-587.

Rundberg, R.S. 1987. *Assessment report on the kinetics of radionuclide adsorption on Yucca Mountain tuff*. Los Alamos National Laboratory. LA-11026-MS, New Mexico.

Russo, R.E., X.L. Mao, O.V. Borisov, and H.C. Liu. 2000. Laser ablation in atomic spectroscopy. *Encyclopedia of Analytical Chemistry: Instrumentation and Applications*. John Wiley & Sons.

Shackelford, C. 1991. Laboratory diffusion testing for waste disposal – A review. *J. Contam. Hydro.*, 7:177-217.

Stewart, G.L. 1972. Clay water interactions, the behavior of ^{3}H and ^{2}H in adsorbed water and the isotope effect. *Soil Sci. Soc. Amer. Proc.*, 36:421-426.

Soeder, D. J., L. E. Flint, and A. L. Flint. 1991. Effects of sample handling and measurement methodology on the determination of porosity in volcanic rock samples, Agronomy Abst.:232. Annual Meeting, Amer. Soc. Agronomy, Madison, WI.

Tokunaga, T. K., and J. Wan. 1997. Water film flow along fracture surfaces of porous rock. *Water Resour. Res.*, 33: 1287–1295.

Tokunaga, T.K., J. Wan, and S.R. Sutton. 2000. Transient film flow on rough fracture surfaces. *Water Resour. Res.*, *36*(7): 1737–1746.

Tokunaga, T.K., K.R. Olson, and J. Wan. 2003. Moisture characteristics of Hanford gravels: Bulk, grain-surface, and intragranular components. *Vadose Zone J.*, 2: 322-329.

Tomutsa, L., D. Doughty, A. Brinkmeyer, and S. Mahmood. 1992. *Imaging techniques applied to the study of fluids in porous media*. NIPER-582. National Institute for Petroleum and Energy Research, Bartlesville, OK.

Triay, I.R., A. Meijer, J.L. Conca, K.S. Kung, R.S. Rundberg, B.A. Strietelmeier, and C.D. Tait. 1997. *Summary and synthesis report on radionuclide retardation for the Yucca Mountain Site Characterization Project*. Milestone 3784M, Los Alamos National Laboratory, Los Alamos.

Wang, J.S.Y., E.L. Hardin, and L.D. Rickertsen. 2001. Crushed tuff as an invert diffusion barrier to enhance waste-isolation capacity. *Proceedings of the 9th International High-Level Radioactive Waste Management Conference*. Las Vegas, Nevada.

Figure Captions

Figure 1 Schematic of different components of water present in an aggregate medium and their effects on diffusion. $D_{Interior}$ and $D_{Surface}$ denote interior and surface diffusion, respectively. (Modified from Conca and Wright, 1992.)

Figure 2 Electrical conductivity measurement cell.

Figure 3 Half-element diffusion experimental setup and schematics of micro-scale mapping. Face number designation is in the center of each face; face 1 and face 6 are the interface and far-side faces, respectively.

Figure 4 Cross-sectional CT images of two sizes of tuff gravel packed inside a column with an inner diameter of 6.22 cm. (a) 16–25 mm tuff gravel. (b). 6.3–9.5 mm tuff gravel. Spatial resolution in the viewed plane is ~ 0.2 mm x 0.2 mm. Voxel depth is 1 mm.

Figure 5 1 mm cross-sectional CT images for 6.3–9.5 mm tuff gravel. (a) under a partially saturated condition. (b) water distribution (wet scan – dry scan).

Figure 6 Diffusion coefficients versus volumetric water content for this and other work. Legend “15 mm tuff, this work (LA/ICP-MS)” includes the coefficients of surface diffusion for bromide in both cubic and tetrahedral sinks (Table 2). Diffusion coefficients reported in Conca and Wright (1992) were for 86 soil and gravel samples, various bentonites, and rock core of tuff basalt and mudstone. The size of crushed tuff and silica sand was not reported in OCRWM (2000a).

Figure 7 Tracer distributions from surface mapping using LA/ICP–MS (100 μm spot size and 10 laser pulses) for cube-cube configuration after diffusion inside nearly 100% RH chamber after 149.7 days. Y-axis: intensity ratio (dimensionless) denotes the signal of each tracer (solid circle: bromide; solid square: perrhenate) divided by the signal of aluminum.

Figure 8 Tracer distributions (200 µm spot size and 20 laser pulses) on the surface of Face 3 for both source (filled symbols) and sink (open symbols) cubes inside (a) 98% RH chamber after 0.79 days and (b) 43% RH chamber after 16.3 days. X-axis: 0 indicates the interface, and increasing positive number indicates increasing distance from the interface in the sink cube.

Figure 9 Relative bromide concentrations in the sink elements from 98% RH experiments. Lines are the fitted analytical diffusion solutions (Equation 1) with the effective diffusion coefficients shown in the legend.

Figure 10 Adsorption isotherm of water on (a) fully hydroxylated quartz; contact angle = 0^o (modified from Gee *et al*., 1990, Figure 1), and (b) heat-dehydroxylated quartz; contact angle = 43^o (modified from Gee *et al*., 1990, Figure 2).

Table 1. Diffusion coefficients and cell conditions during EC measurements.

Tuff grain volumetric water content (cm^3/cm^3)[†]	0.945	0.194	0.118	0.118	0.118	0.114	0.104	0.103	0.097	0.098
Cell volumetric water content[‡]	0.547	0.092	0.055	0.055	0.055	0.052	0.050	0.052	0.049	0.05
Intergranular porosity	0.494	0.494	0.494	0.494	0.494	0.539	0.517	0.495	0.494	0.487
Avg D_e (m^2/s)	6.53E-10	3.46E-11	1.39E-11	1.48E-11	1.36E-11	5.27E-12	2.22E-12	2.03E-12	2.00E-12	1.24E-12

[†] Calculated volumetric water content based on the crushed tuff bulk volume (=volume of water/total volume of tuff grains including intragranular porosity). Values exceeding the grain porosity (0.105) indicate conditions beyond grain saturation.

[‡] Calculated volumetric water content based on the cell volume (=volume of water/cell volume)

Table 2. Experimental conditions and measured diffusion coefficients

Half-element configuration	Relative humidity (%)	Bulk liquid saturation † (%)	Exp. time (d)	Sampling locations	Tracer	Effective diffusion coefficient (m^2/s)	$D_{Br}/D_{Perrherate}$
Cube–Cube	98	88.76	0.79	Surface	Bromide	8.0E-11	1.60
					Perrherate	5.0E-11	
				Interior	Bromide	6.0E-11	1.50
					Perrherate	4.0E-11	
Cube–Tetrahedron	98	71.65	1.14	Surface	Bromide	4.0E-11	1.14
					Perrherate	3.5E-11	
Cube–Cube	93	50.15	16.17	Surface	Bromide	4.0E-11	2.00
					Perrherate	2.0E-11	
				Interior	Bromide	4.0E-11	3.33
					Perrherate	1.2E-11	
Cube–Cube	76	22.93	16.24	Surface	Bromide	1.5E-12	1.88
					Perrherate	8.0E-13	
				Interior	Bromide	1.0E-12	2.50
					Perrherate	4.0E-13	
Cube–Tetrahedron	76	24.47	27.24	Surface	Bromide	5.0E-13	1.25
					Perrherate	4.0E-13	
Cube–Cube	43	7.99	16.28	Surface	Bromide	1.5E-14	1.25
					Perrherate	1.2E-14	
				Interior	Bromide	1.8E-14	1.50
					Perrherate	1.2E-14	
Cube–Tetrahedron	43	4.20	27.32	Surface	Bromide	4.0E-14	2.00
					Perrherate	2.0E-14	

† The value is the bulk liquid saturation for the sink element, and the measured porosity is 0.0827±0.0036 for eight tuff cubes.

Figure 1

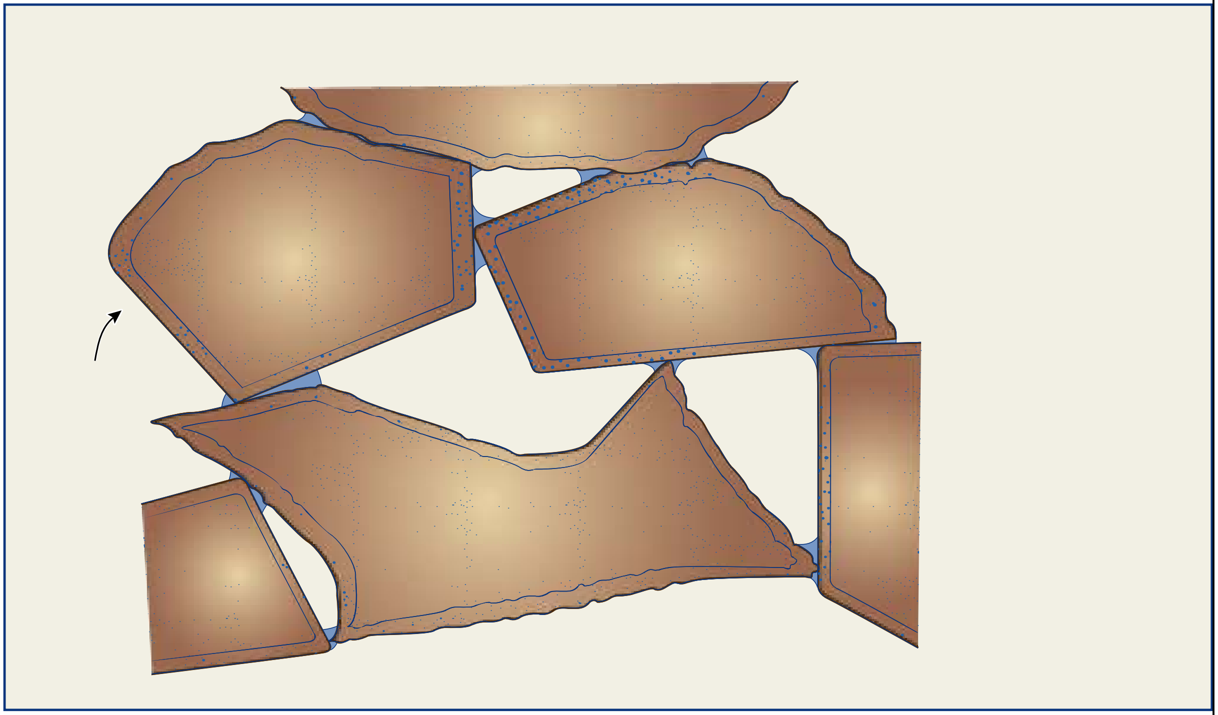

Figure 2

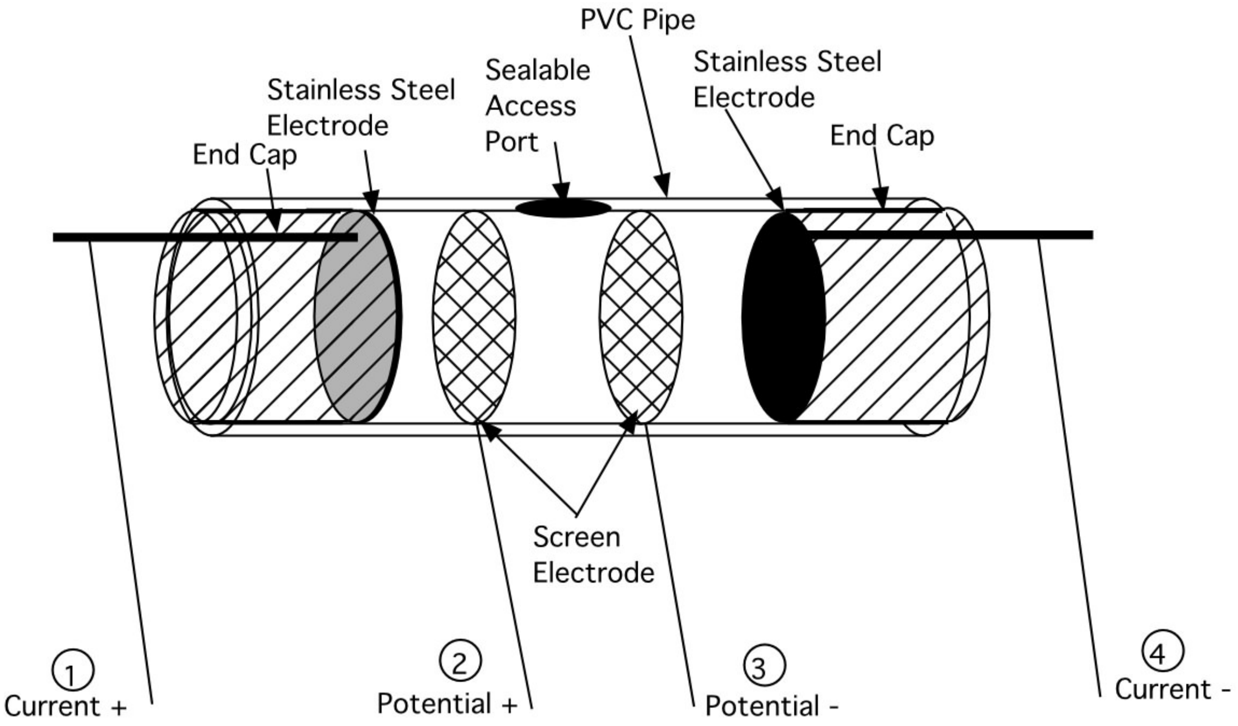
PVC Pipe
Sealable Access Port
Stainless Steel Electrode
End Cap
Stainless Steel Electrode
End Cap
Screen Electrode
① Current +
② Potential +
③ Potential -
④ Current -

Figure 3

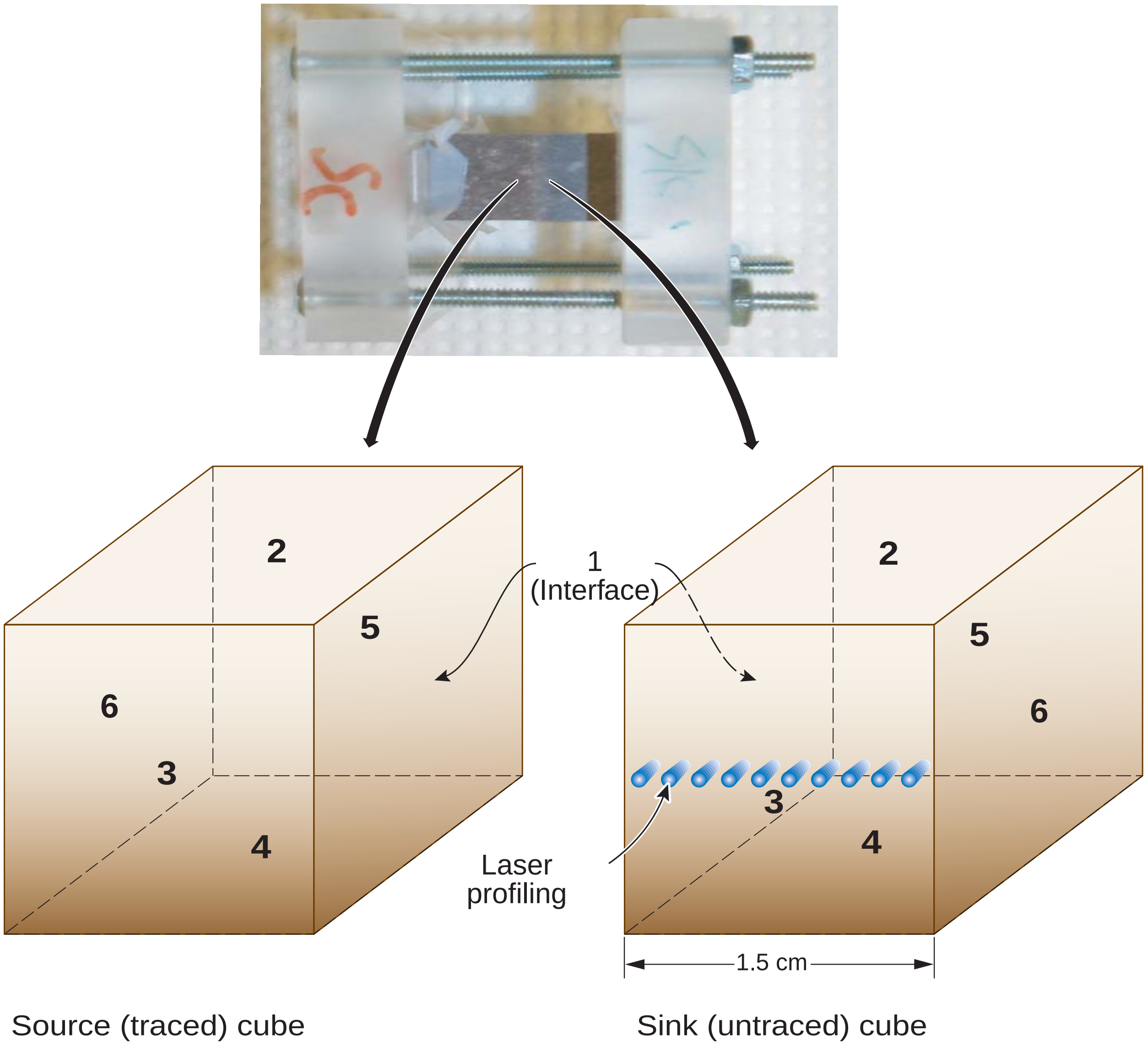
2
5
6
3
4
1
(Interface)
Laser
profiling
2
5
6
3
4
1.5 cm
Source (traced) cube
Sink (untraced) cube

Figure 4

(a)

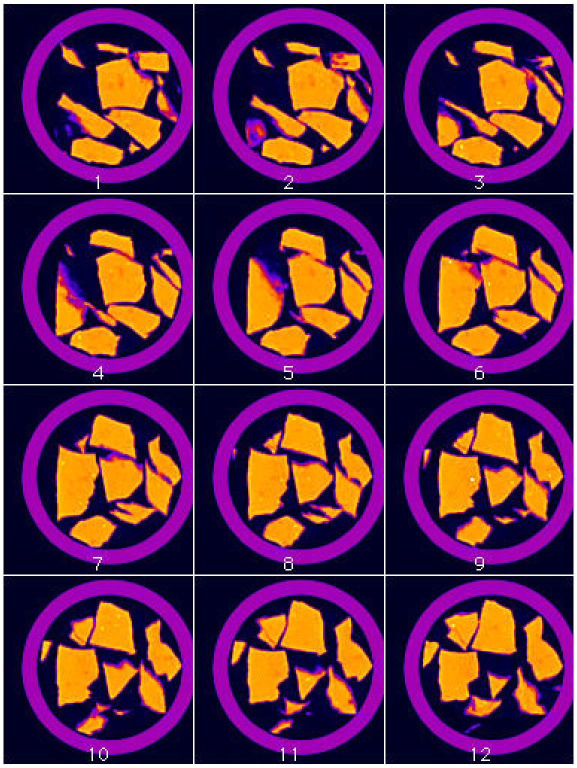

(b)

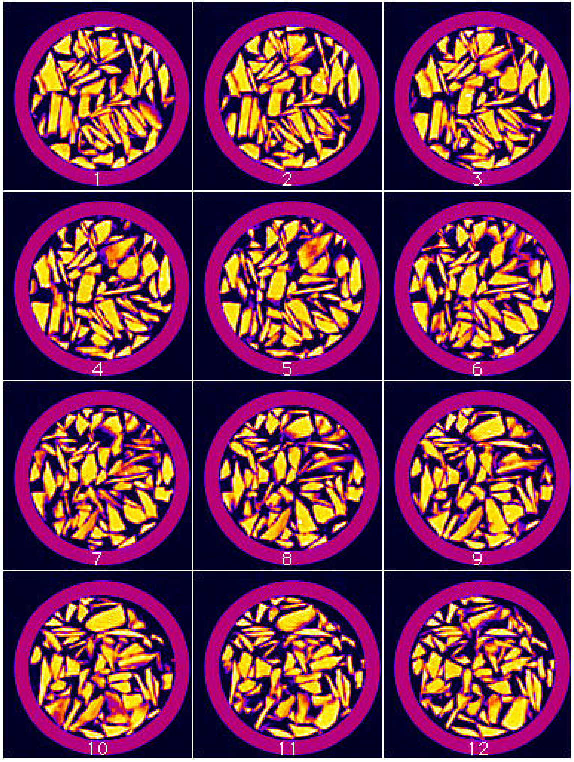

Figure 5

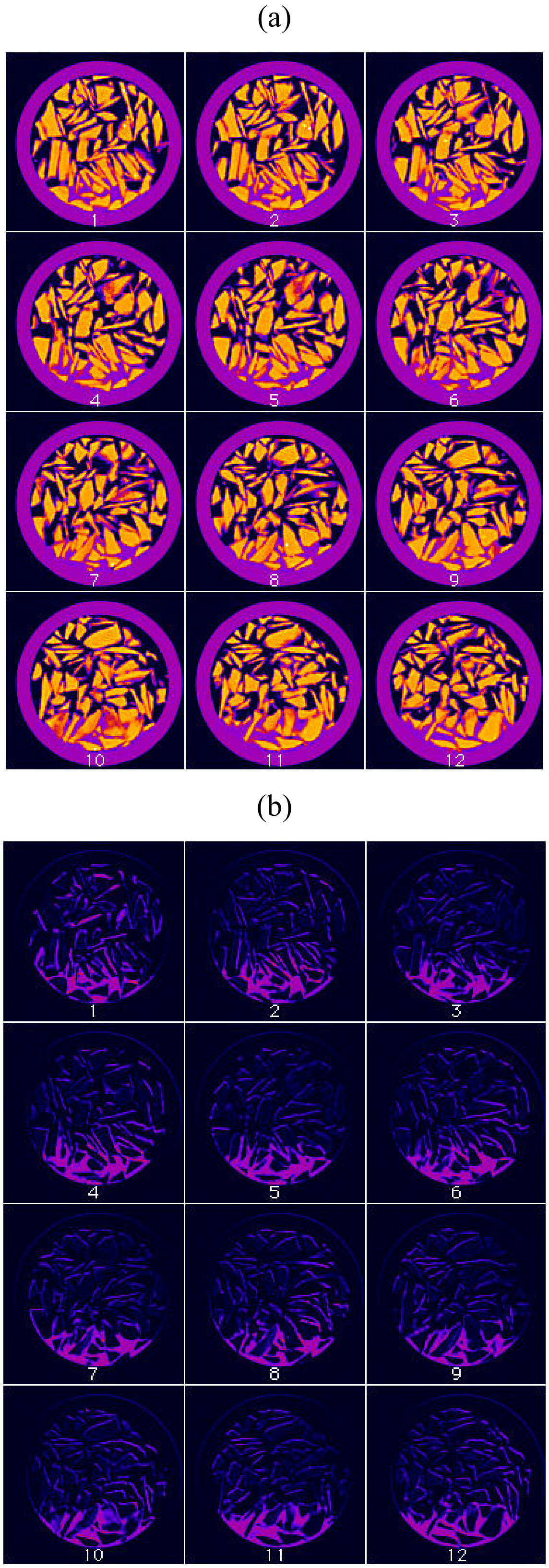

Figure 6

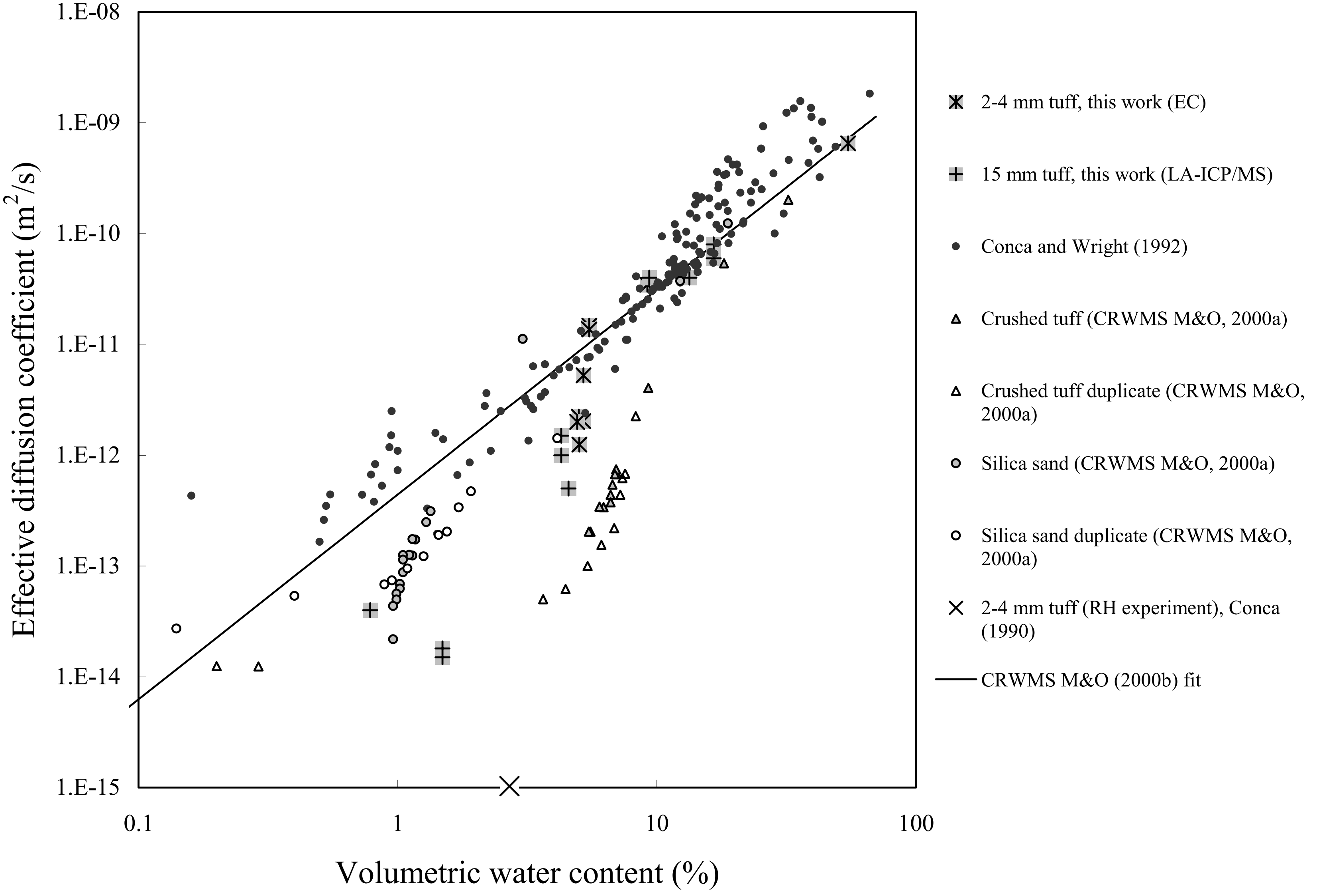
1.E-08
1.E-09
1.E-10
1.E-11
1.E-12
1.E-13
1.E-14
1.E-15
Effective diffusion coefficient (m²/s)
0.1
1
10
100
Volumetric water content (%)
2-4 mm tuff, this work (EC)
15 mm tuff, this work (LA-ICP/MS)
Conca and Wright (1992)
Crushed tuff (CRWMS M&O, 2000a)
Crushed tuff duplicate (CRWMS M&O, 2000a)
Silica sand (CRWMS M&O, 2000a)
Silica sand duplicate (CRWMS M&O, 2000a)
2-4 mm tuff (RH experiment), Conca (1990)
CRWMS M&O (2000b) fit

Figure 7

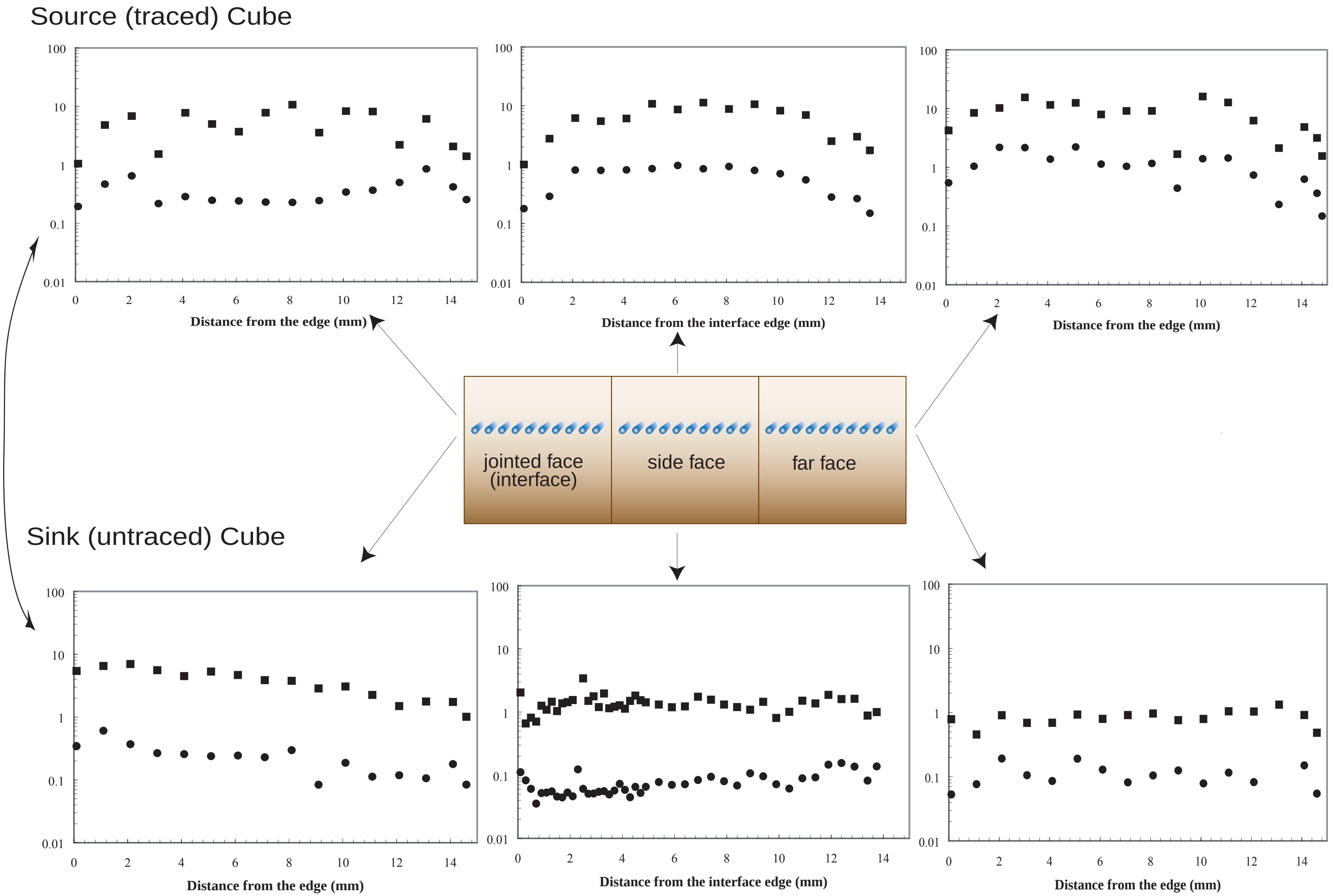
Source (traced) Cube
Sink (untraced) Cube
jointed face (interface)
side face
far face
100
10
1
0.1
0.01
0
2
4
6
8
10
12
14
Distance from the edge (mm)
Distance from the interface edge (mm)

Figure 8

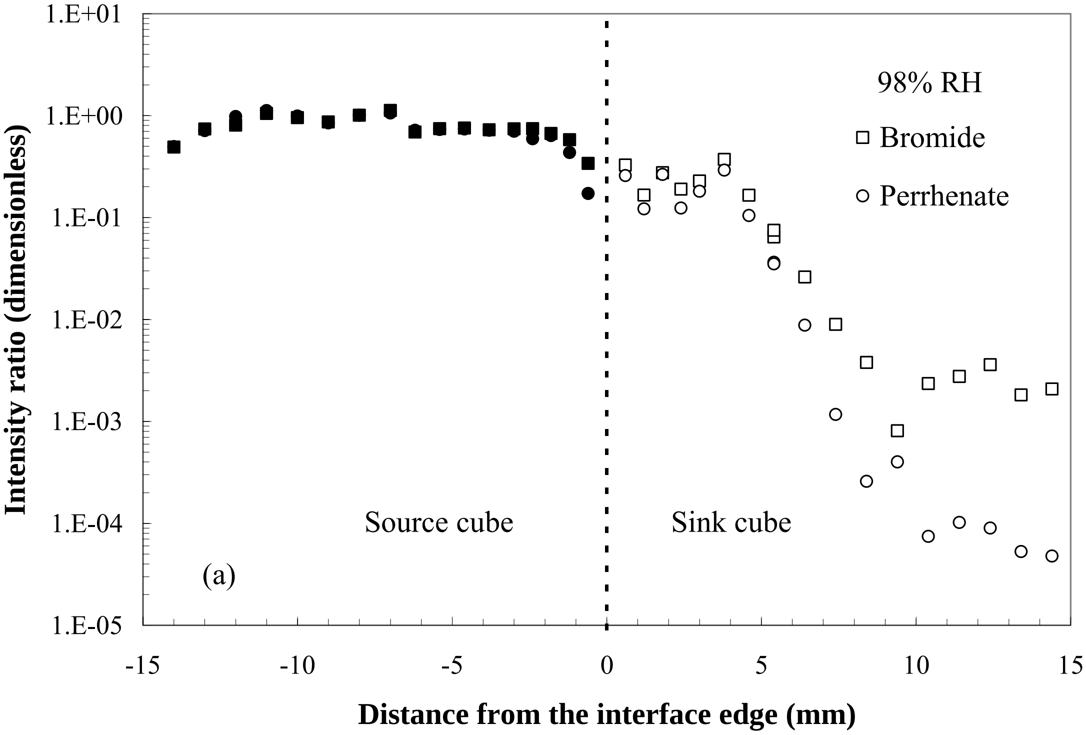
98% RH
□ Bromide
○ Perrhenate
Source cube
Sink cube
(a)
Intensity ratio (dimensionless)
1.E+01
1.E+00
1.E-01
1.E-02
1.E-03
1.E-04
1.E-05
-15
-10
-5
0
5
10
15
Distance from the interface edge (mm)

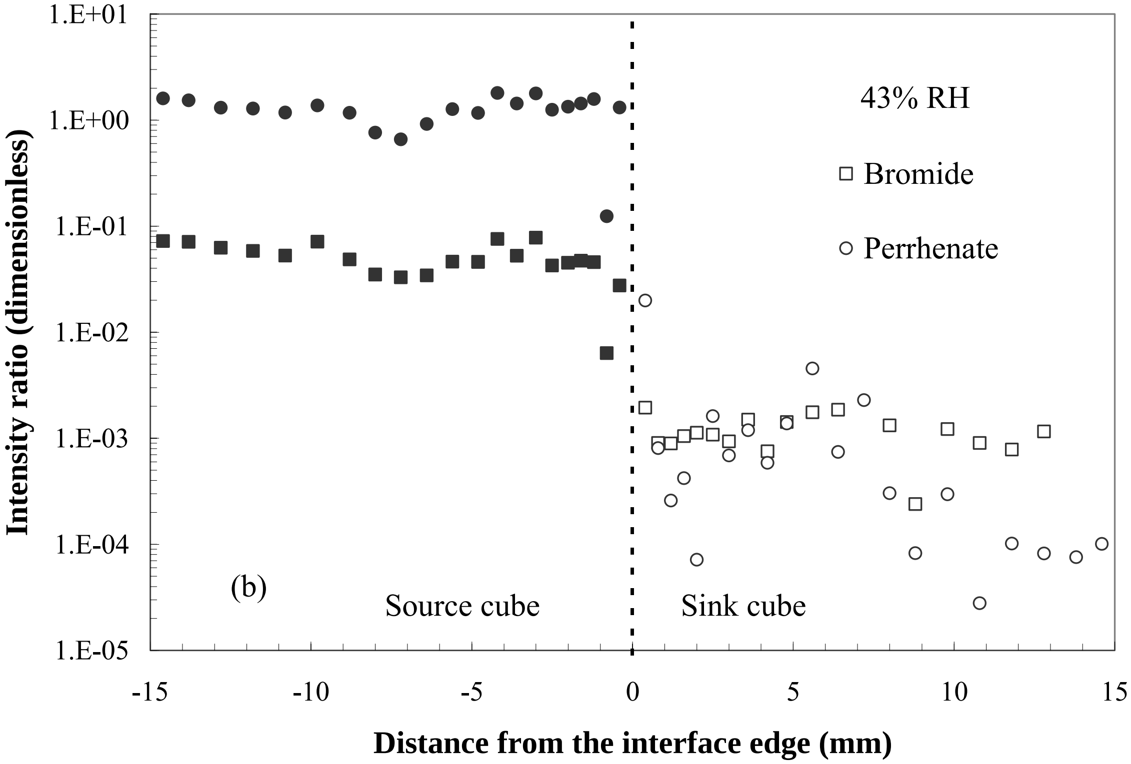
43% RH
□ Bromide
○ Perrhenate
(b)
Source cube
Sink cube
Intensity ratio (dimensionless)
1.E+01
1.E+00
1.E-01
1.E-02
1.E-03
1.E-04
1.E-05
-15
-10
-5
0
5
10
15
Distance from the interface edge (mm)

Figure 9

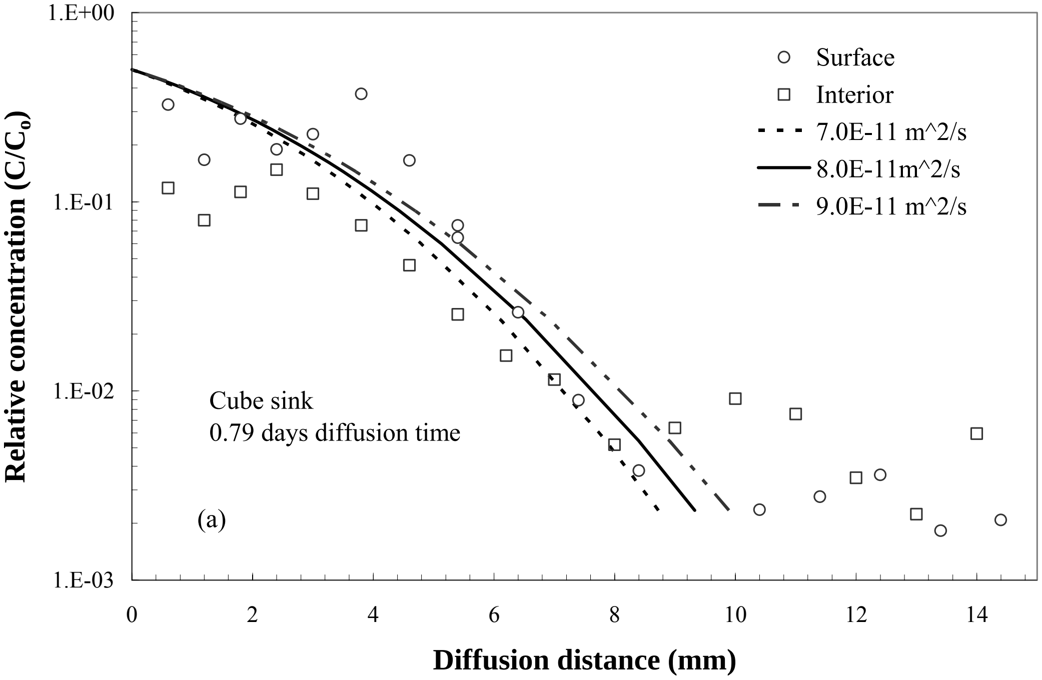
1.E+00
1.E-01
1.E-02
1.E-03
Relative concentration (C/C_0)
0
2
4
6
8
10
12
14
Diffusion distance (mm)
Surface
Interior
7.0E-11 m^2/s
8.0E-11m^2/s
9.0E-11 m^2/s
Cube sink
0.79 days diffusion time
(a)

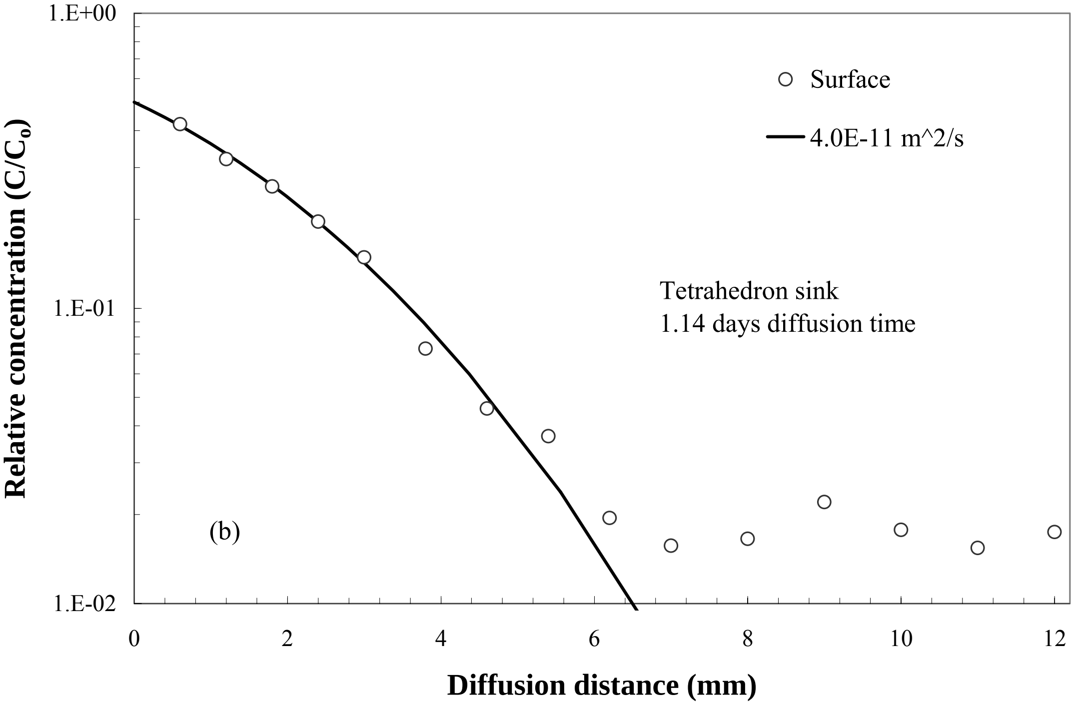
1.E+00
1.E-01
1.E-02
Relative concentration (C/C_0)
0
2
4
6
8
10
12
Diffusion distance (mm)
Surface
4.0E-11 m^2/s
Tetrahedron sink
1.14 days diffusion time
(b)

Figure 10

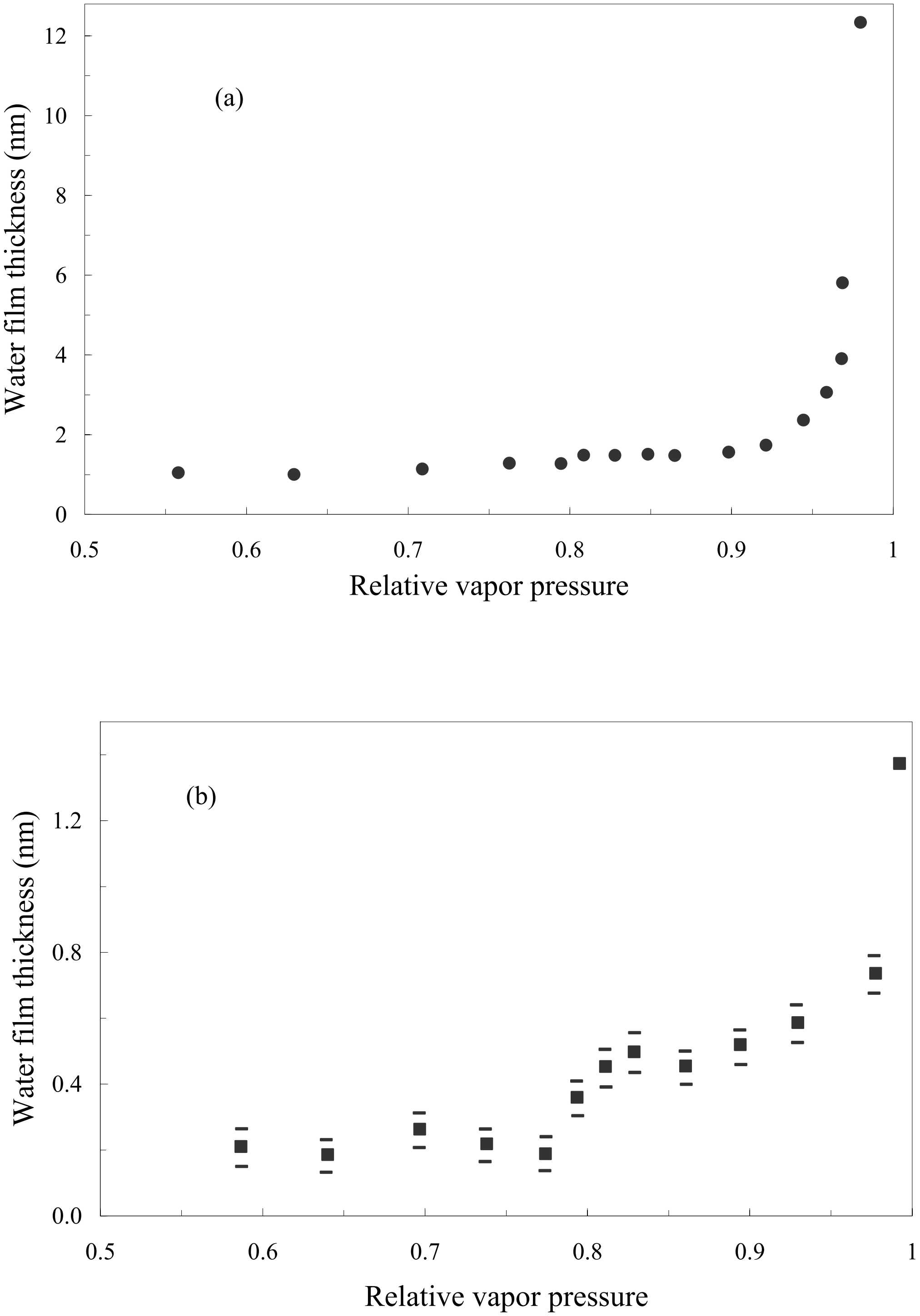
(a)
Water film thickness (nm)
0
2
4
6
8
10
12
0.5
0.6
0.7
0.8
0.9
1
Relative vapor pressure
(b)
Water film thickness (nm)
0.0
0.4
0.8
1.2
0.5
0.6
0.7
0.8
0.9
1
Relative vapor pressure